

# Connectivity Analysis in Clustered Wireless Sensor Networks Powered by Solar Energy

Prodromos-Vasileios Mekikis, *Student Member, IEEE*, Elli Kartsakli, *Senior Member, IEEE*, Angelos Antonopoulos, *Senior Member, IEEE*, Luis Alonso, *Senior Member, IEEE*, Christos Verikoukis, *Senior Member, IEEE*

## Abstract

Emerging 5G communication paradigms, such as machine-type communication, have triggered an explosion in ad-hoc applications that require connectivity among the nodes of wireless networks. Ensuring a reliable network operation under fading conditions is not straightforward, as the transmission schemes and the network topology, i.e., uniform or clustered deployments, affect the performance and should be taken into account. Moreover, as the number of nodes increases, exploiting natural energy sources and wireless energy harvesting (WEH) could be the key to the elimination of maintenance costs, while also boosting immensely the network lifetime. In this way, zero-energy wireless-powered sensor networks (WPSNs) could be achieved, if all components are powered by green sources. Hence, designing accurate mathematical models that capture the network behavior under these circumstances is necessary to provide a deeper comprehension of such networks. In this paper, we provide an analytical model for the connectivity in a large-scale zero-energy clustered WPSN under two common transmission schemes, namely unicast and broadcast. The sensors are WEH-enabled, while the network components are solar-powered and employ a novel energy allocation algorithm. In our results, we evaluate the trade-offs among the various scenarios via extensive simulations and identify the conditions that yield a fully connected zero-energy WPSN.

## Index Terms

Wireless-Powered Sensor Network, Connectivity, Clustered Poisson Process, Battery-less sensors, Solar Harvesting, Zero-Energy Networks, Stochastic Geometry

P.-V. Mekikis is with the Department of Signal Theory and Communications (TSC), Technical University of Catalonia (UPC), Spain, and the University of Athens (UoA), Greece, (e-mail: vmekikis@tsc.upc.edu).

E. Kartsakli is with Iquadrat Informatica S.L., Barcelona, Spain, (e-mail: ellik@iquadrat.com).

L. Alonso is with TSC, UPC, (e-mail: luisg@tsc.upc.edu).

A. Antonopoulos and C. Verikoukis are with the Telecommunications Technological Centre of Catalonia (CTTC), Spain, (e-mail: {aantonopoulos, cveri}@cttc.es).

## I. INTRODUCTION

The upcoming introduction of 5G communication networks is bringing novel communication paradigms, including massive machine-type communication (mMTC) and mission-critical MTC (cMTC), into the spotlight [1]. Full connectivity among large numbers of low-power wireless devices, i.e., the ability of all nodes to reach each other via a multihop path, is of utmost importance to enable high reliability in several fields, e.g., intelligent transportation systems, intrusion detection and industrial process automation [2]. To satisfy these demands in large-scale networks, two issues should be guaranteed: i) High connectivity: ensuring that every node is able to connect to at least one neighbor, thus preventing node isolation, and ii) High availability: the network energy supply should allow for uninterrupted operation, as inoperable nodes could disrupt potential paths that connect parts of the network.

Regarding the first issue, the communication among nodes should be carefully studied and consider both the node deployment and the channel randomness due to fading. Unlike non-fading environments (where the range is deterministic [3]), in fading environments the strongest link may not correspond to the nearest neighbor [4]. This fact demonstrates the significance of the transmission scheme employed in the presence of fading, where the differences in the performance of the unicast (i.e., point-to-point transmission) and broadcast (i.e., point-to-multiple points) schemes could be vast in terms of lifetime and quality of service [5]. Moreover, in many real life scenarios, the wireless sensors operate in clustered formations to exchange messages locally with their proximate devices or gateways (GWs). For instance, smart city sensors are typically clustered in densely populated areas [6] or smart transportation sensors in cars form clusters during traffic hours and exchange data around gateways deployed on traffic lights [7]. Therefore, it is significant to take into account the clustered topology under fading conditions in the performance evaluation, since it affects the generated interference [8].

Another important issue is the network's energy supply, which becomes critical as the network infrastructure grows. During the last few decades, solar energy has been suggested as a promising solution for a sustainable operation in communication networks [9]. By equipping the network infrastructure with solar panels and rechargeable batteries, it is feasible to supply the necessary power throughout a day achieving a zero-energy operation. Also, to avoid power outages caused by low energy intake in worst case conditions, e.g., full cloud cover, smart weather-aware energy

management algorithms that handle the energy allocation efficiently should be designed.

However, although solar energy harvesting is a viable approach for deployments that have sufficient space for the necessary harvesting equipment, it cannot be applied in many applications where the wireless sensors are size-constrained and embedded in places with scarce natural sources. To overcome this issue, Wireless Energy Harvesting (WEH) [10] has been proposed as an effective solution for low-power wireless sensors. In WEH, the energy of radio-frequency (RF) signals is converted to direct current (DC) electricity through a rectenna [11]. In this way, the devices are free to move or even be embedded in walls or human bodies without affecting extensively their ability to replenish their energy. To increase and control the provided wireless energy, dedicated power transmitters or power beacons (PBs) that supply RF energy to the sensors are distributed in the deployment area [12]. Moreover, due to the involvement of a potentially large number of wireless sensors in mMTC and cMTC applications, equipping them with batteries requires high maintenance costs as a result of the inconvenient traditional methods to replenish their energy (i.e., battery replacement or cable-charging). Still, by carefully designing the PB deployment, it is possible to discard the batteries, if the received energy at a temporary storage unit on the node, e.g., a capacitor, is sufficient for sensing, processing and transmitting.

Altogether, there is an extensive body of literature that studies separately the aforementioned topics. More specifically, the connectivity and the effects of the transmission schemes in ad-hoc networks have been investigated in [3]–[5]. However, these works do not consider the topology or the energy supply that affect significantly the network performance. Moreover, the results of various works on solar-powered communication networks [13]–[16] present a great impact on their lifetime, but they do not consider the communication performance. Similarly, although works on the allocation of solar harvested energy [17], [18] manage to prevent power outages in the network, they assume that the communication performance remains unaffected by the changes in the energy intake during the network operation. Furthermore, there are several works on large-scale WEH-enabled networks [12], [19]–[21], but: i) they do not study the network connectivity, which is crucial to ensure that all nodes are able to deliver their messages, and ii) they assume that the network devices, i.e., GWs or PBs, are connected to the electricity grid. Hence, to the best of our knowledge, there is still a gap regarding the joint investigation of the communication performance in zero-energy wireless-powered sensor networks (WPSNs).

In this paper, we study the connectivity performance of zero-energy large-scale networks with

WEH-enabled sensors. We assume a clustered topology where wireless-powered sensors transmit their measurements to solar-powered gateways that exchange this information with the rest of the network under two transmission schemes, i.e., unicast and broadcast. Moreover, the sensors harvest RF power transmitted by a solar-powered PB infrastructure. For the allocation of the harvested energy in PBs and gateways, we employ a novel cloud-aware algorithm in order to achieve a high network connectivity without energy interruptions due to energy limitations. Our contribution can be summarized in the following points:

- We propose an analytical framework that considers solar-powered network devices and WEH-enabled wireless sensors to provide closed-form solutions of: i) the probability of a node to be able to transmit (active) under fading conditions, and ii) the end-to-end connectivity probability for the unicast and the broadcast case.
- We provide a novel weather-aware energy allocation algorithm that adjusts the power transmissions of GWs and PBs. The goal of the algorithm is to provide active network operation throughout a day based on a solar harvesting model that takes into account the solar radiation and the cloud-cover. The experimental data employed for the cloud cover are based on satellite and surface measurements for a 30-year period.
- We conduct an extensive performance assessment, which provides useful insights for the design of zero-energy WPSNs. In our evaluation, we assume realistic solar radiation and cloud patterns for more accurate results.

The rest of the paper is organized as follows. Section II discusses the related work. Section III describes the system model. The analytical modeling of solar and RF energy harvesting are provided in Section IV. Then, in Section V, we provide the analysis on the end-to-end connectivity of the network. Section VI presents the model validation and the simulation results. Finally, Section VII concludes the paper.

## II. RELATED WORK

In this section, we provide a brief literature review of the related work. There are three different fields related to our paper: i) network connectivity analysis, ii) solar-powered networks, and iii) WEH-enabled networks. Thus, we present notable works that have influenced our paper.

To begin with, with the introduction of mission-critical WSN applications, various researchers investigated the probability of full connectivity in ad-hoc networks to identify and prevent the

occasions that a node is isolated from the rest of the network [3], [4]. One of the first works on this subject is [3] in which the connectivity and the impact of mobility in a large set of nodes is investigated. The same topic is extended in [4] by taking the channel randomness into account. In addition, the connectivity in such networks under different transmission schemes is studied in [5]. The ideas of these works are employed and extended in our paper by considering the network topology and the energy supply, which is an important factor for the network sustainability.

Moreover, there are various works that consider solar energy for the energy supply of communication networks. More specifically, in [15], the authors present an algorithm that maximizes the network lifetime with solar harvesting nodes, while the connectivity is guaranteed. Nonetheless, the connectivity is not derived mathematically, but it is given as an optimization constraint, while the channel conditions are not taken into account. Additionally, [16] studies a clustered network in which there are two types of nodes, i.e., wireless-powered sensors and solar-powered clusterheads. The authors propose a framework for the optimal node placement and clusterhead selection to increase the energy efficiency of the network and provide various insights on WSNs powered by hybrid sources. Also, the works in [13], [14] focus on the maximization of solar energy intake by optimizing the solar energy harvesting system, while assuming that each wireless sensor node is equipped with its own solar harvesting module. In addition, another issue that affects the lifetime of solar-powered networks and has been studied recently is the energy allocation. Various risk-averse algorithms have been suggested for this task [17], [18]. In [17], the authors employ neural networks for the prediction of the solar energy arrivals and they focus entirely on the optimization of solar energy intake. Also, [18] focuses on the minimization of the grid energy consumption by taking into account the power allocation.

Furthermore, WEH-enabled large-scale networks have gained a lot of attention lately [12], [19]–[21]. Many of these works, i.e., [19], [20], discuss various network metrics, e.g., spatial throughput and coverage, but not the probability of connectivity, which guarantees the reliability of safety-critical applications. It is worth mentioning that [19] is among the first works that consider battery-less WEH-enabled devices. Obviously, this requires very low power devices, but it has been shown that it is possible using appropriate protocols, e.g., harvest-then-transmit. Also, [12] provides a comprehensive study on deploying PBs in cellular networks to achieve infinite node lifetime and eliminate the need of power cords. This technique is employed in our paper in order to increase the network reliability. Moreover, the connectivity in a WPSN is

studied in [21], where various insights are given on the design of such networks. However, the infrastructure is powered by the electricity grid, without any consideration on the sustainability of the network. Consequently, motivated also by [22] in which wireless-powered communications are surveyed, we undertook the task to combine solar-powered network devices with WEH-enabled nodes in our connectivity analysis.

### III. SYSTEM MODEL

#### A. Network and Channel Model

We consider a network deployed on the Euclidean plane that consists of three types of entities:

- Gateways (GWs): We model the random sensor locations according to a Poisson cluster process. Therefore, the parent point process represents the clusterheads (gateways) of each cluster and it is modeled by a homogeneous Poisson point process (PPP)<sup>1</sup>  $\Phi_g = \{g_1, g_2, \dots\}$  with intensity  $\lambda_g$ , where  $g_i, \forall i \in \mathbb{N}$ , denotes the location (i.e., Cartesian coordinates) of the  $i^{\text{th}}$  clusterhead. The purpose of each gateway is to receive measurements from sensors and deliver/exchange them to/with another part of the network. Thus, the existence of at least one path between every pair of GWs is essential.
- Sensors: As in many real life scenarios [6], [7], we assume that the wireless sensors operate in clustered formations. Hence, each parent point is surrounded by a Poisson distributed number of interferers with a mean number  $\bar{n}$  (i.e., active sensors on average), distributed around each clusterhead according to a symmetric normal distribution with variance  $\sigma^2$  and a density function

$$f(x) = \frac{1}{2\pi\sigma^2} \exp\left(-\frac{\|x\|^2}{2\sigma^2}\right). \quad (1)$$

Each sensor attempts to deliver its measurements to the gateway (clusterhead), which then communicates with the other gateways to exchange information collected by their sensors.

- Power Beacons (PBs): On the same plane, we deploy the PBs that transfer energy to the sensors in order to achieve a battery-less operation. As in [12], the PBs are represented by a homogeneous PPP  $\Phi_b = \{y_1, y_2, \dots\}$  with intensity  $\lambda_b$ , where  $y_j, \forall j \in \mathbb{N}$ , denotes the location of the  $j^{\text{th}}$  PB.

<sup>1</sup>Poisson point processes are prominently employed for the mathematical modeling of various types of communication networks, such as cellular networks and WSNs [23], [24].

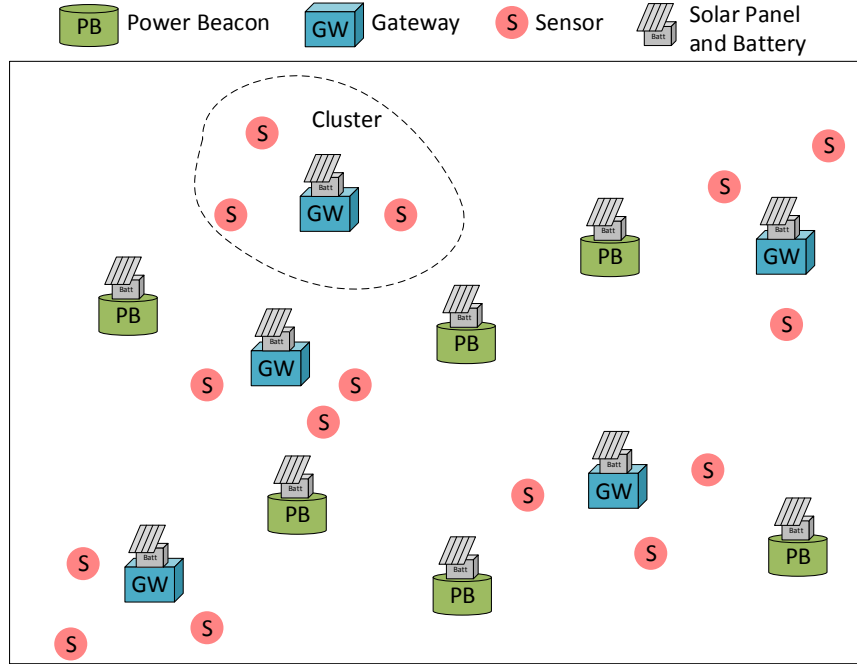


Fig. 1: Network topology.

In Fig. 1, we demonstrate all the network entities and the topology of our network.

In our analysis, we examine the ability of a sensor to connect to the gateway of its cluster, based on the received power denoted as  $P_{rx} = P_{tx}hr^{-\alpha}$ , where  $P_{tx}$  is the sensor transmission power,  $r$  is the distance between the gateway and its transmitter,  $\alpha$  is the path loss exponent and  $h$  is the fast fading power coefficient, which is independent and identically distributed (i.i.d.). For this reason, the amplitude fading  $\sqrt{h}$  is Rayleigh distributed, i.e., ideal for outdoor scenarios, with a scale parameter  $\sigma = 1$ , thus  $h$  is exponentially distributed with mean value  $\mu = 1$ . In different scenarios, other distributions for the fading could be employed, such as Rice or Nakagami [25]. Each gateway experiences interference from the other active sensors inside the cluster, as well as from the other clusters. Therefore, a sensor is considered connected with its gateway (i.e., is able to deliver a message), when the received signal to interference ratio (SIR) is higher than a threshold  $\gamma$ , as it is given in

$$\text{SIR} = \frac{P_{tx} \cdot h \cdot r^{-\alpha}}{I_{intra} + I_{inter}} \geq \gamma, \quad (2)$$

where  $r$  is the Euclidean distance between the two nodes,  $I_{intra}$  denotes the interference from the other nodes of the same cluster and  $I_{inter}$  denotes the interference received from the active nodes of the other clusters.

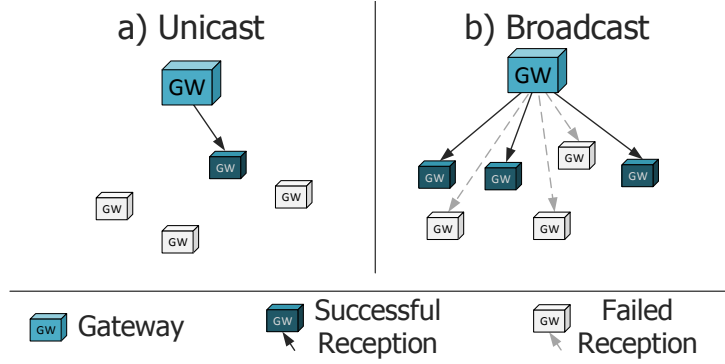


Fig. 2: Transmission schemes.

Regarding the gateway communication, we consider two transmission mechanisms:

- **Unicast:** In the first scenario, we study the unicast mechanism, in which a GW is considered connected only if the nearest neighbor can decode successfully the transmitted message.
- **Broadcast:** In the second scenario, a gateway broadcasts its message and it is considered connected if at least one of the receivers is able to decode the message, regardless of its proximity to the source node.

The two transmission mechanisms are illustrated in Fig. 2.

### B. Energy Harvesting Model

To ensure that the sensors will always have enough energy to operate, they employ the harvest-then-transmit protocol with which the nodes harvest energy from the PBs for a certain period of time and then consume all of it for measurement and communication [19]. To that end, time is divided into two periods:

- The harvesting period (HP) that consists of  $S$  time slots, in which all sensors accumulatively harvest RF energy from the PBs with RF-to-DC conversion efficiency  $\epsilon$ .
- The communication period (CP) which has a duration of 1 slot. In the CP slot, the sensors with sufficient harvested energy (active) transmit their messages to the GW of their cluster.

A sensor is considered active during the CP if, at the end of the HP, it has received and stored temporarily, e.g., at a capacitor,  $\theta$  Joules from the PBs that enables it to transmit a message with power  $P_{tx}$ . We assume that  $\theta = P_{tx}t_{tx} + \delta$ , where  $\delta$  is the energy margin for other operations, e.g., sensing and processing, and  $t_{tx}$  is the duration of the sensor transmission in seconds. Hence, at the end of the transmission, the stored energy of active nodes is depleted, as the  $\theta$  threshold guarantees enough energy for only one transmission.

Set 1	Active	Active	Active	Active	Active	Active
Set 2	Idle	Active	Idle	Active	Idle	Active
Set 3	Idle	Idle	Active	Idle	Idle	Active
HP #	1	2	3	4	5	$\xi=6$

Fig. 3: Status of the node sets for  $\nu = 3$ .

Furthermore, we consider that inactive nodes store their energy and wait for the following HPs to reach the  $\theta$  threshold. To take this issue into account, we assume that the nodes are separated into  $\nu$  different sets, according to their ability to harvest the required energy in  $\nu$  HPs. For instance, if  $\nu = 2$ , then we have two sets: i) one set consists of the nodes that harvest enough energy in one HP, and ii) the other set consists of all the rest of the sensors that need two HPs to harvest enough energy. The CP in which all sets will be concurrently active occurs after  $\xi$  HPs, i.e., a hyperperiod, which is the least common multiple of all the natural numbers from 1 to  $\nu$ . To that end, we can calculate the number of HPs needed to ensure that all sets of nodes will be eventually active. In Fig. 3, we depict an operational example for  $\nu = 3$ , where we observe three sets of nodes. Set 1 will manage to harvest enough energy in every HP, while the second set will harvest the required energy every two HPs and set 3 every three HPs. As we may observe, in this case, the whole WPSN will be active after  $\xi = 1 \cdot 2 \cdot 3 = 6$  HPs and, after that, a new hyperperiod starts.

Moreover, we assume that all PBs and GWs are connected to a rechargeable battery of capacity  $L_f$  powered by a solar panel of size  $A$  m<sup>2</sup> with solar panel efficiency  $\eta$  and performance ratio  $r_p$ . The gateways transmit with a power  $P_g$  that depends on the harvested solar energy and varies between a minimum (i.e., that satisfies the minimum communication requirements) and maximum value (i.e., respecting the higher limits of the FCC's Code of Federal Regulations [26]), denoted as  $P_g^-$  and  $P_g^+$ , respectively. For similar reasons, the transmission power  $P_b$  of the PBs varies between  $P_b^-$  and  $P_b^+$ . Also, when active, GWs and PBs consume power  $P_{g,idle}$  and  $P_{b,idle}$  for the rest functions of the device, e.g., processing. For reliability reasons, the infrastructure is also connected to the electricity grid, to avoid a power outage in worst-case conditions.

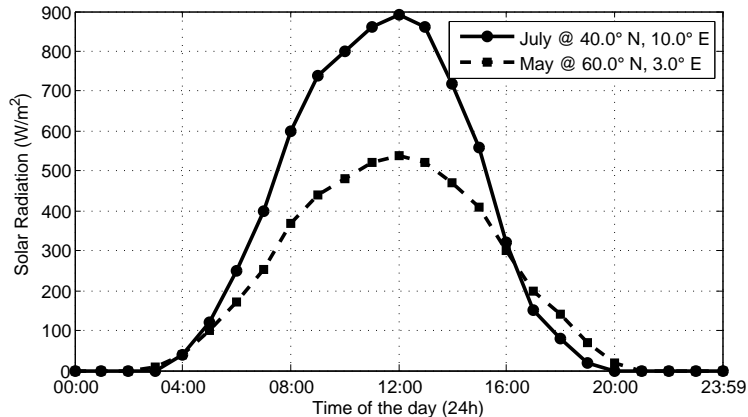


Fig. 4: Solar Radiation vs. Time of the day at two random locations on earth. Data source: [27]

#### IV. ENERGY HARVESTING

In this section, we present the mathematical derivations for the energy harvesting models that will be employed to acquire the network connectivity. First, we formulate the solar harvesting model and explain the risk-averse energy allocation algorithms for the PBs and gateways. Then, we provide the derivations of the probability of active node for the RF harvesting sensor nodes.

##### A. Solar Harvesting

The general formula to estimate the energy generated in a solar panel of area  $A$ , efficiency  $\eta$  and performance ratio  $r$  is given by

$$\text{Energy} = \text{SR} \cdot r_p \cdot \eta \text{ kWh}, \quad (3)$$

where SR denotes the solar radiation (measured in  $\text{W}/\text{m}^2$ ), which depends on the time, the location, the orientation and the inclination of the panel relative to the sun. A typical solar radiation pattern at two random locations on earth is shown in Fig. 4 for the duration of one day. From this figure, we can notice that the solar radiation data for every day follows a quadratic relation to the time of the day. As it is also suggested in [28], we can take advantage of this characteristic in order to formulate a radiation model for every month by employing quadratic fitting. To that end, the power  $H$  generated at a solar panel with surface  $A \text{ m}^2$  can be described by

$$H = A(\chi(t + \psi)^2 + \omega), \quad (4)$$

where  $\chi$ ,  $\psi$  and  $\omega$  are the fitting parameters for the quadratic curve of each month. Also,  $t \in \{0, 23\}$  denotes the time.

Although this model is accurate to measure the solar panel power output in a clear sky, it

does not consider the fraction of the sky obscured by clouds. In order to have a more realistic solar harvesting model, we should take into account the cloud cover for the chosen area, as it affects significantly the solar panel performance. In fact, the energy acquired from a solar panel in a cloudy weather is complex and can fluctuate due to shading or edge-of-cloud effects, i.e., cumulus clouds reflect and concentrate sunlight, magnifying its power. However, as our goal is the average performance of the network, the fluctuations would be averaged out. Therefore, we employ [29] for the cloud distribution, which is an accurate and tractable solution for the cloud cover. More specifically, the cloud cover distribution can be characterized by the Beta distribution defined on the interval  $[0, 1]$  with probability density function (PDF) given by

$$f(x) = \frac{\Gamma(\alpha + \beta)}{\Gamma(\alpha)\Gamma(\beta)} x^{\alpha-1} (1-x)^{\beta-1}, \quad (5)$$

and expected value  $\mathbb{E}[X] = \alpha/(\alpha + \beta)$ , where  $\alpha, \beta > 0$  are the shape parameters that control the shape of the distribution. It should be noted that many works extend [29] by providing a cloud cover analysis (i.e.,  $\alpha$  and  $\beta$  parameters) for specific regions around the world. For instance, [30] provides the shape parameters in Europe based on satellite and surface cloud cover observations for a 30-year period. The shape parameters of the Beta distribution can be adjusted for every season according to the region in which the city under investigation falls in (see Table II).

Thus, by taking into account the Beta distributed random variable (RV)  $CC \sim \text{Beta}(\alpha, \beta)$  for the cloud cover, (4) turns into

$$H = A(\chi(t + \psi)^2 + \omega)(1 - CC(t, \alpha, \beta)). \quad (6)$$

The roots of (6) define the time of the day that the solar panel starts and stops harvesting energy, i.e., the time that the sun rises and sets, denoted as  $t_r$  and  $t_s$ , respectively, provided by

$$t_r = \left( -\psi - \sqrt{-\frac{\omega}{\chi}} \right) \text{ and } t_s = \left( -\psi + \sqrt{-\frac{\omega}{\chi}} \right). \quad (7)$$

Therefore, the total amount of energy harvested from a solar panel in one day is given by

$$H_{\text{total}} = (1 - CC(t, \alpha, \beta)) \int_{t_r}^{t_s} A(\chi(t + \psi)^2 + \omega) dt, \quad (8)$$

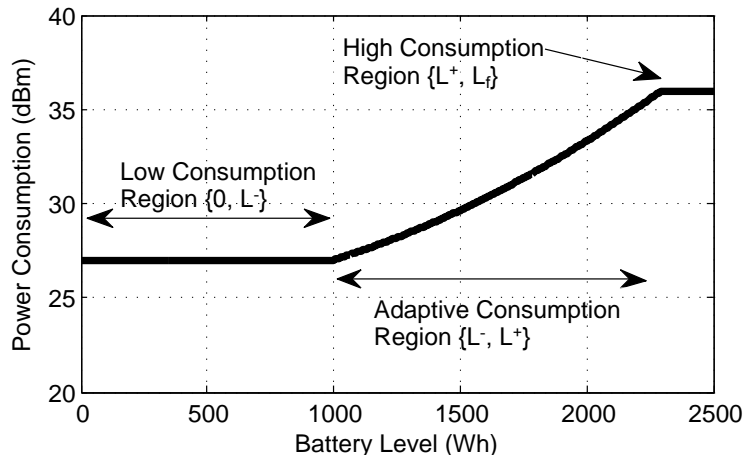


Fig. 5: The cost function  $U$  vs. the battery level  $L$ .

while the energy stored in the battery in one hour is

$$H_h(t) = (1 - CC(t, \alpha, \beta)) \int_t^{t+1} A(\chi(t + \psi)^2 + \omega) dt, \quad (9)$$

for  $t_r < t < t_s - 1$ . These equations can assist in designing energy allocation algorithms that consider the harvesting performance.

1) *Cloud-Cover-Aware Risk-Averse Algorithm*: In order to achieve a green and uninterrupted network operation, we need to design an algorithm that handles the received energy while it considers the sky conditions and the amount of time that the system will not be able to harvest energy. For this reason, we provide Algorithm 1 that minimizes the risk of power outages by adjusting the power consumption of the devices (i.e., GWs and PBs) in real-time, based on the available information, i.e., battery level and history of cloud cover.

In the beginning of Algorithm 1, we provide the necessary parameters for the energy allocation to the network infrastructure. For simplicity, we assume a common notation for PBs and GWs. Therefore, the power consumption for the devices varies between  $P^+$  and  $P^-$ . Regarding the battery, it is required to know its current level ( $L$ ) and its total capacity ( $L_f$ ). Also, we consider two thresholds for the battery level, an upper denoted as  $L_+$  and a lower denoted as  $L_-$ .

We assume saturated conditions where gateways always have data to transmit and that the

---

**Algorithm 1: Cloud-Cover-Aware Algorithm for Energy Allocation**


---

**Input :** Battery Level  $L(t)$  with thresholds  $L_+$  and  $L_-$ , Battery Capacity  $L_f$ , Power consumption limits  $P^+$  and  $P^-$ , Operation period  $\Pi$ , Shape parameters  $\alpha$  and  $\beta$ .

**Output:** Transmission power  $P_b = U(t) - P_{b,idle}$  for PBs and  $P_g = U(t) - P_{g,idle}$  for GWs, Electricity grid connections

```

1 Initialize time  $t = 1$ ;
2 Initialize battery level  $L(t) = L_f$ ;
3 while  $t < \Pi$  do
4   Calculate prediction for current cloud cover  $CC(t, \alpha, \beta) \sim \text{Beta}(\alpha, \beta)$ ;
5   Calculate harvested energy  $H_h(t) = (1 - CC(t, \alpha, \beta)) \int_t^{t+1} A(\chi(t + \psi)^2 + \omega) dt$ ;
6   if  $H_h(t) > 0$  then
7     if  $L(t) > L_+$  then
8       | Set  $U(t) = P^+$ ;
9     else if  $L(t) \leq L_-$  then
10      | Set  $U(t) = P^-$ ;
11     else
12      | Calculate previous cloud cover  $CC(t-1) = \left(1 - \frac{L(t) - L(t-1) + U(t-1)}{\int_{t-1}^t A(\chi(t + \psi)^2 + \omega) dt}\right)$ ;
13      | Set  $U(t) = \max\left(P^-, \frac{P^+(L^2 - L_-^2) - P^-(L^2 - L_+^2)}{(L_+^2 - L_-^2)(1 - (CC(t-1) + CC(t, \alpha, \beta))/2)^{-1}}\right)$ ;
14      end
15    else
16      if  $L(t) > L_+$  then
17        | Set  $U(t) = P^+$ ;
18      else if  $L(t) \leq L_-$  then
19        | Set  $U(t) = P^-$ ;
20      else
21        | Calculate mean cloud cover  $\mathbb{E}_{day}(CC) \sim \alpha/(\alpha + \beta)$ ;
22        | Set  $U(t) = \max\left(P^-, \frac{P^+(L^2 - L_-^2) - P^-(L^2 - L_+^2)}{(L_+^2 - L_-^2)(1 - \mathbb{E}_{day}(CC))^{-1}}\right)$ ;
23        end
24      end
25    if  $H_h(t) \geq P^-$  AND  $L(t) \geq P^-$  then
26      | Set grid(off);
27      | Set  $L(t+1) = \min\{L(t) - U(t) + H_h(t), L_f\}$ ;
28    else
29      | Set grid(on);
30      | Set  $L(t+1) = \min\{L(t) + H_h(t), L_f\}$ ;
31    end
32    Set  $t = t + 1$ ;
33 end

```

---

cost function that defines the power consumption for the following hour is given by

$$U(t) = \begin{cases} P^+, & \text{if } L > L_+ \\ \max\left(P^-, \frac{(L_+^2 - L_-^2)^{-1}(P^+(L^2 - L_-^2) - P^-(L^2 - L_+^2))}{(1 - (CC(t-1) + CC(t, \alpha, \beta))/2)^{-1}}\right), & \text{if } L_- < L \leq L_+ \text{ \& } H_h(t) > 0 \\ \max\left(P^-, \frac{P^+(L^2 - L_-^2) - P^-(L^2 - L_+^2)}{(L_+^2 - L_-^2)(1 - \mathbb{E}_{day}(CC))^{-1}}\right), & \text{if } L_- < L \leq L_+ \text{ \& } H_h(t) = 0 \\ P^-, & \text{if } L \leq L_- \end{cases} \quad (10)$$

To that end, the allocated energy is chosen in real-time between the minimum and maximum transmission power when the battery level is lower than  $L_-$  or higher than  $L_+$ , respectively. On the other hand, when  $L_- < L \leq L_+$ , the allocation algorithm follows the trend of a quadratic equation, as depicted in Fig. 5. For instance, in this example, when the battery level is between  $L_- = 1000$  and  $L_+ = 2300$ , the allocated energy follows (10) to smooth the power consumption. Furthermore, in order to increase the accuracy of the algorithm, when  $L_- < L \leq L_+$ , the algorithm calculates the cloud cover for the cost function of the next hour based on both the Beta distribution and the actual solar panel shading of the current hour. Consequently, even in the case that the solar panel is covered by objects other than clouds, the algorithm will be able to adjust the consumption accordingly. Moreover, during the night, (10) takes into account the mean cloud cover, i.e.,  $\mathbb{E}_{day}(CC) \sim \alpha/(\alpha + \beta)$ , in order to adapt the consumption based on the expected cloud cover of the season. After this, we verify that the harvested or the stored energy will provide a viable operation to power the system; otherwise, it sets the electricity grid on.

It should be noted that preventing a power outage using the cloud-cover-aware algorithm does not mean that the communication performance will be unaffected. In order to achieve the least possible connections to the electricity grid, Algorithm 1 reduces the transmission power of the infrastructure resulting in longer HPs for the sensors and, thus, possible delays in the communication. Nevertheless, this is an essential step towards zero-energy networking.

### B. Wireless Energy Harvesting

In order to investigate whether a sensor node has sufficient power to transmit at the end of the  $\nu^{th}$  HP, we have to calculate the active node probability  $p_a$ , which determines the number  $S$  of harvesting slots in an HP needed for all nodes to become active after  $\nu$  HPs. In the following proposition, we present the derivations for the probability  $p_a$ .

**Proposition 1.** *The probability that a node is active is given by*

$$p_a = \operatorname{erf}\left(\frac{\lambda_b \Gamma(S + \frac{1}{2})}{2\Gamma(S)} \sqrt{\frac{\pi^3 \nu P_b \epsilon}{\theta}}\right), \quad (11)$$

where  $\operatorname{erf}(z) = \frac{2}{\sqrt{\pi}} \int_0^z e^{-t^2} dt$ .

*Proof.* First, we derive the active node probability  $p'_a$  in the absence of fading by considering the accumulated received power from the set of the PBs and calculate the probability that this

amount is higher than the threshold  $\theta$ . We also consider that some nodes will require  $\nu$  HPs to surpass this threshold. Hence, we obtain

$$p'_a = \mathbb{P}\left(S \cdot \sum_{j=1}^q \epsilon P_b |y_j|^{-\alpha} \geq \frac{\theta}{\nu}\right) = \quad (12)$$

$$= \mathbb{P}\left(\sum_{j=1}^q |y_j|^{-\alpha} \geq \frac{\theta}{\nu S \epsilon P_b}\right), \quad (13)$$

where the sum in (12) is the total harvested power from PBs at a node located at the origin<sup>2</sup>,  $P_b$  is given from Algorithm 1 and  $|y_j|$  denotes the Euclidean distance between the  $j^{\text{th}}$  PB and the origin.

To calculate (13), we have first to focus on the distribution of the sum  $Y = \sum |y|^{-\alpha}$  and derive its characteristic function  $F_I(\omega) = \mathbb{E}(e^{j\omega Y})$ . According to [23], by conditioning on having  $k$  nodes in a disk of radius  $\rho$  and then de-conditioning on the Poisson number of nodes, while letting  $\rho$  go to infinity, we obtain

$$F_I(\omega) = \exp(-\lambda_b \pi \Gamma(1 - 2/\alpha) \omega^{2/\alpha} e^{-j\pi/\alpha}), \quad (14)$$

where  $\Gamma(t) = \int_0^\infty x^{t-1} e^{-x} dx$  is the gamma function.

It can be noticed that (14) is a stable distribution with shift 0, skew 1, stability  $2/\alpha$  and scale  $(\lambda_b \pi \Gamma(1 - 2/\alpha) \cos(\pi/\alpha))^{\alpha/2}$ . Therefore, the complementary cumulative distribution function (CCDF) in (13) can be found as an infinite series [33]

$$p'_a = \sum_{k=1}^{\infty} \frac{\Gamma(2k/\alpha)}{\pi k!} \left( \frac{\lambda_b \pi \Gamma(1 - 2/\alpha)}{(\frac{\theta}{\nu S P_b \epsilon})^{2/\alpha}} \sin(k\pi(1 - 2/\alpha)) \right)^k. \quad (15)$$

For the special case of  $\alpha = 4$ , (14) reduces to a Lévy distribution with shift 0 and scale  $\pi^3 \lambda_b^2 / 2$ , yielding

$$p'_a = \text{erf}\left(\frac{\pi^{\frac{3}{2}} \lambda_b}{2} \sqrt{\frac{\nu S P_b \epsilon}{\theta}}\right). \quad (16)$$

Moreover, to calculate  $p_a$  in the presence of fading, we have to follow a similar approach as in  $p'_a$ . Therefore, the probability  $p_a$  that the harvested power after  $S$  slots and  $\nu$  HPs is higher

<sup>2</sup>Conditioning on a point at the origin does not affect the statistical properties of the coexisting PPP according to Slivnyak's theorem [31].

than a threshold  $\theta$  is given by

$$p_a = \mathbb{P}\left(\epsilon P_b \cdot \sum_{j=1}^q (|y_j|^{-\alpha} h_1 + \dots + |y_j|^{-\alpha} h_S) \geq \frac{\theta}{\nu}\right) = \mathbb{P}\left(\sum_{j=1}^q \left(|y_j|^{-\alpha} \sum_{t=1}^S h_t\right) \geq \frac{\theta}{\nu \epsilon P_b}\right). \quad (17)$$

It should be noted that the sum of the fading exponential RVs follows an Erlang distribution,  $h_1 + \dots + h_S = \sum_t H_t \sim \text{Erlang}(S, 1)$ , as it is also noted in [19]. Then, we calculate the Laplace transform of the sum in (17) that will lead to the distribution of the harvested energy. Thus, following [23, 5.1.7], we obtain

$$\mathcal{L}(s) = \mathbb{E}\left(\prod_{j \in \Phi_b} \exp(-s|y_j|^{-\alpha} H_t)\right) = \exp\left(-\lambda_b \pi \mathbb{E}(H^{2/\alpha}) \Gamma(1 - 2/\alpha) s^{2/\alpha}\right), \quad (18)$$

which is a stable distribution and, when  $\alpha = 4$ , the Lévy CCDF is given by

$$F(x) = \text{erf}\left(\frac{\pi \lambda_b \mathbb{E}(H^{2/\alpha})}{2} \sqrt{\frac{\pi}{x}}\right). \quad (19)$$

By taking the mean value of the Erlang variable  $\mathbb{E}(H^{2/\alpha}) = \frac{\Gamma(S + \frac{2}{\alpha})}{\Gamma(S)}$  and replacing  $x$  with  $\frac{\theta}{\nu \epsilon P_b}$  (see (17)), we conclude the proof.  $\square$

Using the results from Proposition 1, we can derive the number  $S$  of harvesting slots needed to achieve a certain probability  $p_a$ .  $S$  is essential for calculating the required amount of time needed to achieve a fully active network, i.e.,  $p_a = 1$ .

**Lemma 1.** *The number of harvesting slots required to achieve a given  $p_a$  probability is given by*

$$S = \frac{\theta}{\nu P_b \epsilon} \left( \frac{2 \text{erf}^{-1}(p_a)}{\pi^{\frac{3}{2}} \lambda_b} \right)^2. \quad (20)$$

*Proof.* In the non fading case, calculating  $S$  from (16) is straightforward by solving this equation for  $S$ . However, it is not as simple for the fading case and we have to treat (11) differently, as the gamma functions complicate the procedure. Nevertheless, we can replace these functions by employing the asymptotic series for the gamma function given by

$$\Gamma(S) = e^{-S} S^{S-1/2} \sqrt{2\pi} \left( 1 + \frac{1}{12S} + \frac{1}{288S^2} + \dots \right). \quad (21)$$

Then, using the derivations provided in Appendix A, we obtain the following formula

$$\frac{\Gamma(S + \frac{1}{2})}{\Gamma(S)} \approx \sqrt{S}, \quad (22)$$

which can be replaced in (11), leading to the following result

$$p_a = \operatorname{erf}\left(\frac{\lambda_b \sqrt{S}}{2} \sqrt{\frac{\nu \pi^3 P_b \epsilon}{\theta}}\right). \quad (23)$$

This means that the approximated solution for the probability  $p_a$ , given in (23), is exactly the same as the case without fading conditions in  $p'_a$ , given in (16). To that end, solving (23) by  $S$ , yields

$$S = \frac{\theta}{\nu P_b \epsilon} \left( \frac{2 \operatorname{erf}^{-1}(p_a)}{\pi^{\frac{3}{2}} \lambda_b} \right)^2, \quad (24)$$

which holds for both (16) and (11).

This result is important as it demonstrates that even though fading can deteriorate the connectivity of a node, which we will notice in the following section, it does not affect its ability to harvest energy from PBs.  $\square$

## V. END-TO-END CONNECTIVITY

In this section, we will derive the network connectivity by employing the results from Section IV. In order to calculate the end-to-end connectivity, we have first to ensure that the sensors in each cluster are able to deliver their data to their gateway (cluster coverage) and, then, that each gateway is able to communicate these measurements to the rest of the network. In that way, we will investigate the ability of the network to be fully connected and each gateway to have at least one neighbor that will be able to receive its data, ensuring that there are no isolated GWs, i.e., GWs unable to deliver their messages [3]–[5].

### A. Cluster Coverage

In this section, we provide the probability  $p_c$  that a gateway has successfully received a message from an active sensor in its cluster. A sensor message is correctly received by the gateway, when two events hold: i) the sensor has collected sufficient energy (i.e., is active), and ii) the received signal at the gateway to surpass the decoding threshold  $\gamma$ . To that end, the probability  $p_c$  is given by the following lemma.

**Lemma 2.** *The probability that an active sensor node has successfully delivered a message to the gateway is given by*

$$p_c = p_a \int_0^\infty \mathcal{L}_{intra}(\gamma r^\alpha) \mathcal{L}_{inter}(\gamma r^\alpha) f_R(r) dr, \quad (25)$$

where  $\mathcal{L}_{intra}(s)$  is the interference from the other sensors of the cluster,  $\mathcal{L}_{inter}(s)$  is the tight bound of the interference from the sensors of other clusters and  $f_R(r, \sigma^2) = \frac{r}{\sigma^2} \exp\left(-\frac{r^2}{2\sigma^2}\right)$  is the probability density function (PDF) of the distance between the sensor and the gateway.

*Proof.* The proof of Lemma 2 is provided in Appendix B. □

### B. Connectivity

Since we have derived the probability  $p_c$ , we can calculate the probability that each gateway can communicate with the rest in order to have full connectivity in the network. As it is important to define the employed transmission mechanism, we study the connectivity for the unicast and broadcast transmission mechanisms separately, as discussed in Section III.

1) *Unicast:* In the unicast case, the end-to-end connectivity  $\mathcal{C}_{uc}$  is defined by the ability of the gateway to decode a message from an active sensor in its cluster and then to connect with their nearest neighbor. The derivations of  $\mathcal{C}_{uc}$  are given in the following proposition.

**Proposition 2.** *The probability of end-to-end connectivity of a WPSN for the unicast case, denoted as  $\mathcal{C}_{uc}$ , is given by*

$$\mathcal{C}_{uc} = p_c q_{uc} = p_c \left[ \frac{\pi^{\frac{3}{2}} \lambda_g \operatorname{erfc}\left(\frac{\pi \lambda_g \sqrt{P_g}}{2\sqrt{\gamma W}}\right)}{2e^{\frac{-\pi^2 \lambda_g^2 P_g}{4\gamma W}} \sqrt{\frac{\gamma W}{P_g}}} \right]^m. \quad (26)$$

*Proof.* We denote with  $q_{uc}$  the connectivity probability of the gateways. According to [32], if the number of nodes  $m$  is high enough, then

$$q_{uc} = \mathbb{P}(d_{min} \geq 1), \quad (27)$$

where  $d_{min}$  denotes the minimum node degree which is the sum of connections of the node with the fewest connections.

In order to determine if the minimum node degree of the network is equal or higher than one (i.e., full connectivity), we need to calculate the probability that all nodes are connected with at least their nearest neighbors. Assuming statistically independent wireless links, this probability

is

$$q_{uc} = \mathbb{P}(d_{min} \geq 1) = \mathbb{P}(\text{SNR} \geq \gamma)^m = \mathbb{P}\left(hr^{-\alpha} \geq \frac{W\gamma}{P_g}\right)^m. \quad (28)$$

This is a joint probability distribution of the independent RVs  $h$  and  $r$ . Therefore, we have

$$q_{uc} = \mathbb{P}\left(h \geq \frac{r^\alpha W\gamma}{P_g}\right)^m = \quad (29)$$

$$= \left(\int_0^\infty \int_{\frac{y^\alpha W\gamma}{P_g}}^\infty f_h(x)f_r(y)dx dy\right)^m = \quad (30)$$

$$= \left(\int_0^\infty \int_{\frac{y^\alpha W\gamma}{P_g}}^\infty 2\pi\lambda_g y e^{-\pi\lambda_g y^2} e^{-x} dx dy\right)^m \quad (31)$$

$$= \left(\int_0^\infty 2\pi\lambda_g y e^{-\pi\lambda_g y^2} e^{-\frac{y^\alpha W\gamma}{P_g}} dy\right)^m, \quad (32)$$

where (30) follows from the joint distribution of independent variables and (31) follows from the probability density function (PDF) of the distance  $r$  of a node to its nearest active neighbor  $f_R(r) = 2\lambda_g\pi r e^{-\lambda_g\pi r^2}$  [23] and the PDF of an exponential variable with mean value 1. The integral in (31) can be solved either by employing the modified Gauss-Hermite quadrature as in [5] or by assuming  $\alpha = 4$ , which yields

$$q_{uc} = \left(\frac{\pi^{\frac{3}{2}}\lambda_g e^{-\frac{\pi^2\lambda_g^2 P_g}{4\gamma W}} \text{erfc}\left(\frac{\pi\lambda_g\sqrt{P_g}}{2\sqrt{\gamma W}}\right)}{2\sqrt{\frac{\gamma W}{P_g}}}\right)^m. \quad (33)$$

Multiplying (33) with (25), concludes the proof.  $\square$

2) *Broadcast*: In the broadcast case, the connectivity  $\mathcal{C}_{bc} = p_c \cdot q_{bc}$  is defined by the ability of a gateway to connect with any neighbor, regardless of the distance between them, and it is provided by the following proposition.

**Proposition 3.** *The probability of connectivity for the broadcast scheme, denoted as  $\mathcal{C}_{bc}$ , is given by*

$$\mathcal{C}_{bc} = p_c \left[1 - e^{-\frac{\lambda_g\pi^{\frac{3}{2}}}{2}\sqrt{\frac{P_g}{\gamma W}}}\right]^m. \quad (34)$$

*Proof.* Again, to calculate the connectivity probability, we have first to derive the probabilities  $p_c$  and  $q_{bc}$ . However, in this case,  $p_c$  is given by (25), while to calculate the connectivity probability of the gateways  $q_{bc}$ , we have to follow a different approach. According to [4], the isolation

probability for an active node, while considering the channel randomness is given by

$$\mathbb{P}_I = e^{-\lambda_g \pi \mathbb{E}[R^2]}, \quad (35)$$

where  $R$  is the random variable of the communication range. Furthermore,

$$\mathbb{E}[R^2] = \int_0^\infty 2r \mathbb{P}\left(l(r) \geq \frac{W\gamma}{P_g}\right) dr = \quad (36)$$

$$= \int_0^\infty 2r \int_{\frac{W\gamma}{P_g}}^\infty r^\alpha e^{-r^\alpha h} dr dh = \quad (37)$$

$$= \int_0^\infty 2r e^{-\frac{r^\alpha W\gamma}{P_g}} dr = \left(\frac{2}{\alpha}\right) \Gamma\left(\frac{2}{\alpha}\right) \left(\frac{\gamma W}{P_g}\right)^{-\frac{2}{\alpha}}. \quad (38)$$

Eq. (37) follows after considering that the path loss  $l(r)$  is an exponential RV with mean value  $r^{-\alpha}$  [37]. By substituting (38) to (35), the probability  $q_{bc}$  for the broadcast case is given by

$$q_{bc} = (1 - \mathbb{P}_I)^m = \left(1 - e^{-\frac{2\lambda_g \pi}{\alpha} \Gamma\left(\frac{2}{\alpha}\right) \left(\frac{\gamma W}{P_g}\right)^{-2/\alpha}}\right)^m. \quad (39)$$

To that end, by multiplying (39) for  $\alpha = 4$  with  $p_c$ , we obtain the end-to-end connectivity probability in the broadcast case.  $\square$

## VI. PERFORMANCE EVALUATION

In this section, we validate the proposed theoretical framework via extensive simulations and provide useful insights on the use of solar and wireless energy harvesting by comparing the metrics of interest for the different transmission schemes. The simulation environment is developed in Matlab R2014a.

### A. Simulation Setup

We consider the topology shown in Fig. 1 and calculate the connectivity among  $m = 100$  gateways that are surrounded by a given number of sensors (i.e., at any given moment, one of them is the transmitter while the rest are considered interferers) and, thus, we show  $p_c$  for two cases: i) one interferer per cluster, i.e.,  $n = 1$ , and ii) two interferers per cluster, i.e.,  $n = 2$ . In each iteration, we deploy the PBs and GWs randomly and calculate the network performance for this instance. Then, after 10.000 iterations, we calculate and compare the average network performance with our analytical results. Unless otherwise stated, the decoding threshold

TABLE I:  
SIMULATION PARAMETERS

Simulation Parameter	Symbol	Value
Path loss exponent	$\alpha$	4
Threshold ratio	$\gamma$	-10 dB
Sensor transmission power	$P_{tx}$	10 dBm
PB Transmission power	$P_b$	[26, 36] dBm
PB Idle power consumption	$P_{b,idle}$	2.5 W
GW Transmission power	$P_g$	[26, 36] dBm
GW Idle power consumption	$P_{g,idle}$	2.5 W
HP Slots	$S$	5
Energy margin in $\theta$	$\delta$	$2 \cdot 10^{-3}$ Joule
Sensor transmission duration	$t_{tx}$	0.1 s
RF-to-DC conversion efficiency	$\epsilon$	70%
Interferers	$n$	[1, 2] per cluster
GW Intensity	$\lambda_g$	0.01 per m <sup>2</sup>
PB Intensity	$\lambda_b$	[0, 0.05] per m <sup>2</sup>
Scale parameter	$\sigma$	10
Battery Capacity	$L_f$	2000 Wh
Battery level thresholds	$\{L^-, L^+\}$	{1000, 1700} Wh
Solar Panel Area	$A$	0.5 m <sup>2</sup>
Simulation Area	$A_s$	$5 \cdot 10^6$ m <sup>2</sup>

is assumed fixed at  $\gamma = -10$  dB, the number of HPs is  $\nu = 1$ , while the intensity of the clusters and PBs is 0.01 and 0.04 per m<sup>2</sup>, respectively, as shown in Table I. The transmission power of the PBs that power the sensors via WEH varies between 26 and 36 dBm, respecting the limits of the FCC's Code of Federal Regulations [26]. Also, the solar panel efficiency is  $\eta = 0.1$  and its performance ratio is set at  $r_p = 0.75$ . Regarding the sensors, we consider characteristics from real low-power devices [35], [36]. Thus, their data rate is 250 kb/s, while the message that carries its measurement is 20 bytes long (i.e., 8 bytes payload and 12 bytes headers). To that end, the time duration that the sensor is active is 100 ms, i.e., approximately 80 ms for transmission and the rest for processing and measuring. Moreover, the transmission power of the nodes is set at 10 dBm, while the board power consumption due to the processing from the MCU and the measuring from the sensing devices is approximately 8 mA. Consequently, the energy margin  $\delta$  that defines the  $\theta$  threshold is 2 mJ.

*Solar harvesting model setup:* Regarding the solar harvesting model, let us recall that the solar radiation parameter in (3) is measured in W/m<sup>2</sup> and it depends on the time, the location of the panel relative to the sun, its orientation and its inclination. As the solar radiation patterns vary significantly for different areas, it is more practical to choose a specific area to formulate

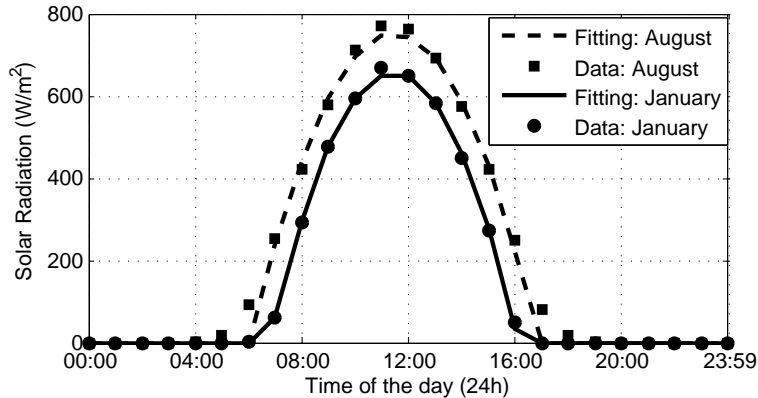


Fig. 6: Solar Radiation vs. Time at Barcelona, Spain for two random days of January and August.

TABLE II: PARAMETERS  $\chi$ ,  $\psi$  AND  $\omega$  FOR THE QUADRATIC SOLAR PANEL POWER OUTPUT MODEL AND BETA PARAMETERS  $\alpha$ ,  $\beta$  FOR THE CLOUD COVER IN BARCELONA, SPAIN

Month	$\chi$	$\psi$	$\omega$	$\alpha$	$\beta$	Region [30]
January	-2.26	-11.4	50	1	0.95	II
February	-1.75	-11.34	45.4	1	0.95	II
March	-1.74	-11.6	45.5	0.9	0.59	II
April	-1.86	-11.45	53.4	0.9	0.59	II
May	-1.79	-11.53	53	0.9	0.59	II
June	-1.57	-11.46	49.5	0.96	2.55	IV
July	-1.84	-11.58	55.9	0.96	2.55	IV
August	-1.93	-11.47	56.4	0.96	2.55	IV
September	-1.75	-11.48	48.7	1.15	1.02	IV
October	-1.79	-11.52	46.5	1.15	1.02	IV
November	-1.74	-11.44	37.7	1.15	1.02	IV
December	-1.89	-11.52	38.9	1	0.95	II

the solar harvesting model. To that end, we assume that our network is located at Barcelona, Spain, which is a densely populated urban area and we employ the solar radiation data from [34, Table 1(b)] for a  $45^\circ$  inclination and a south orientation. Using the aforementioned data, we confirm in Fig. 6 that the solar radiation follows a quadratic behavior versus the time in a day and we show this for two random days in January and August. As we can see, during August the solar radiation is higher as the day lasts longer and the sun is closer to the northern hemisphere in contrast to January. To that end, by employing quadratic fitting on the data from [34], the solar radiation can be described by (4) where  $\chi$ ,  $\psi$  and  $\omega$  are the fitting parameters for the quadratic curve of each month, given in Table II.

To account for the cloud cover, we follow the analysis in [29] regarding the Beta distribution. Hence, we employ measurements from [30], where the author derives the shape parameters

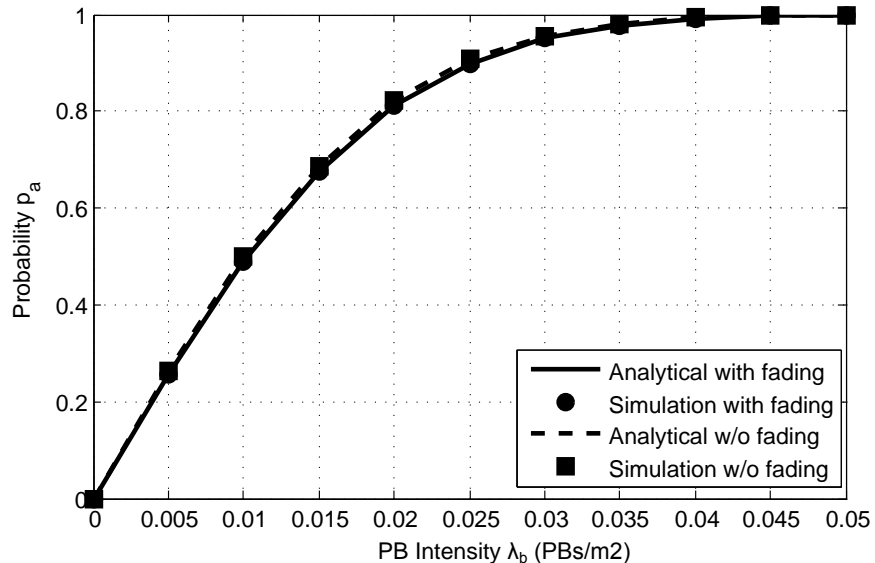


Fig. 7: Probability  $p_a$  vs. PB intensity  $\lambda_b$  for different fading cases. Parameters:  $S = 5$ ,  $P_b = 30$  dBm and  $\nu = 1$ .

$\alpha, \beta > 0$  for the Beta distribution in different cloud cover regions of Europe. The data are based on satellite and surface cloud cover measurements for a 30-year period. To that end, the shape parameters  $\alpha$  and  $\beta$  of the Beta distribution and the region where the area under investigation falls in for each month are given in Table II. Thus, we have all the required information to provide an accurate estimation of the solar panel power output for every hour of the day.

### B. Energy Harvesting Performance Evaluation

In order to validate the analytical derivations of Section IV, we present in Fig. 7 the probability of active node  $p_a$  with and without fading versus the intensity  $\lambda_b$  of the PBs for  $S = 5$ ,  $P_b = 30$  dBm and  $\nu = 1$ . As we may observe, all results show a perfect match with the theory. Moreover, we notice that both cases perform similarly, as it is expected according to Lemma 1. Furthermore, as the intensity of the PBs is rising, the probability  $p_a$  increases as the average distance between a sensor and a PB is decreasing. However, we notice that, for  $\lambda_b > 0.04$ , the probability  $p_a$  saturates. Therefore, for the given HP duration and transmission power, the intensity of the PBs should not exceed the  $0.04$  PBs/m<sup>2</sup>, as it does not offer any benefit in the network performance.

Moreover, in Fig. 8, we employ Lemma 1 to present the relation between the harvesting slots  $S$  and the intensity of the PBs given that the probability  $p_a$  is fixed at  $0.99$  for  $\nu = 1$ . In this way, this figure demonstrates three different  $\lambda_b$  configurations between the harvesting slots  $S$  and

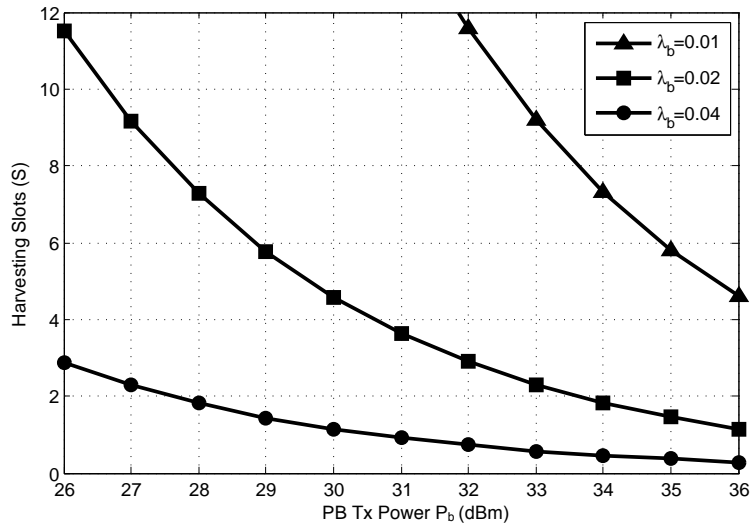


Fig. 8: Harvesting slots  $S$  required to achieve  $p_a = 0.99$  vs. PB transmission power for different PB intensities.

the PB transmission power  $P_b$  that guarantee active operation from approximately all nodes for different density scenarios. As we can see, the number of harvesting slots decreases by increasing either the transmission power or the intensity of the PBs. We also notice that by doubling the PB density, results in smaller HPs (i.e., faster recharge cycles), than doubling the transmission power. For instance, doubling the intensity at  $P_b = 33$  dBm from 0.01 to 0.02, reduces the slots from approximately 9 to only 2. On the other hand, increasing the power transmission from 33 to 36 dBm for the same PB density ( $\lambda_b = 0.01$ ), results to 5 harvesting slots. Thus, mission-critical applications that demand low delay and active operations from all nodes (i.e., mMTC and cMTC) should be designed with a focus on higher PB densities.

However, in cases where the probability  $p_a$  cannot be close to 1, the inactive sensors in the first HP will harvest energy from the following HPs until they are able to transmit, i.e., the  $\theta$  threshold is surpassed. To that end, in order to evaluate the performance of the network when  $p_a < 1$  for  $\nu = 1$ , we demonstrate in Fig. 9, the probability  $p_a$  during a hyperperiod, i.e., the least common multiple of all the natural numbers from 1 to  $\nu$ , given that  $p_a$  reaches 1 when  $\nu = 3$ . Therefore, the hyperperiod has a duration of  $\xi = 6$  HPs and the probability  $p_a$  varies according to Fig. 9. After the first HP,  $p_a$  is around 0.9, but in the last HP of the hyperperiod, approximately all (99%) nodes will be active. It is interesting to notice that, after the fifth HP, the probability  $p_a$  drops to the same level as in the first HP, since only the nodes that are able

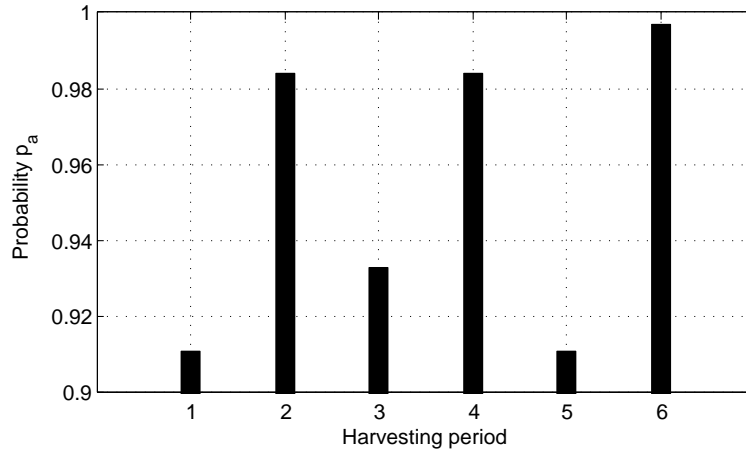


Fig. 9: Probability  $p_a$  during a hyperperiod of  $\nu = 3$ .

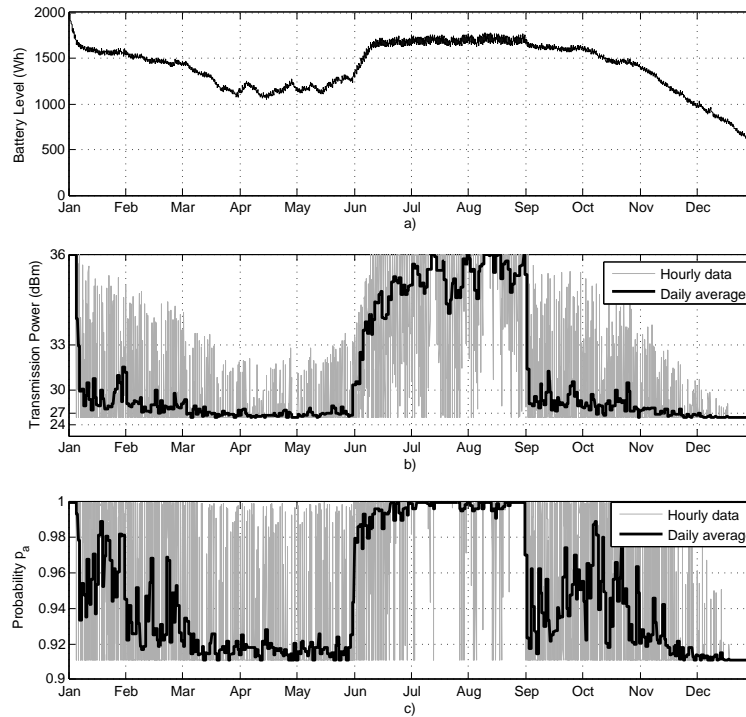


Fig. 10: Performance of the energy allocation algorithms in one year: a) Battery level, b) Transmission Power, c) Active node probability.

to harvest energy in one HP will be active.

Next, in order to demonstrate the variations of the active node probability due to the solar energy harvesting variations, we present, in Fig. 10, the performance of the proposed energy allocation algorithm over the span of one year, i.e., the algorithm begins on January 1 (assuming full battery) and finishes on the 31st of December. As we can see in Fig. 10a, the battery level

drops during the winter months (i.e.,  $\sim 500$  Wh or  $\sim 25\%$ ), but still the algorithm keeps a battery level that prevents any power outage or connection with the electricity grid by decreasing the power transmission, shown in Fig. 10b. Also, we notice that, during the summer months, the battery level increases close to the battery capacity and, as there is abundance of energy in the battery, the transmission power is increased. However, even then (August), the transmission power is decreased in some cases due to high cloud cover, i.e., despite the high battery level, extensive cloud cover provokes a slight decrease in  $P_B$  to reduce the energy consumption. As expected, the probability  $p_a$ , shown in Fig. 10c, follows the trends of the transmission power and we notice that it is over 0.87 throughout the year, which means that at least 87% of the nodes will manage to transmit from the first HP, while the rest will need more HPs to receive the required energy to transmit (see Fig. 9). We should also notice that although employing the proposed energy allocation algorithm reduces vastly the risk of power outage, it sacrifices the communication performance due to the lower  $p_a$  in worst case conditions, i.e., low battery level and/or high cloud cover.

### C. Communication Performance Evaluation

Regarding the communication part, in Fig. 11, we present the cluster coverage probability versus the decoding threshold for two cases, i.e., when there is one or two interferers in a cluster. Apparently, higher  $\gamma$  implies lower coverage probability, as the received signal is not strong enough to be decoded compared to the interference. Also, the same conclusion is reached when the number of interferers is increasing, as the interference becomes stronger at the receiver.

In Fig. 12, we study the end-to-end connectivity versus the PB intensity, while taking into account both the active nodes and the cluster coverage. In this figure, we present the performance of both transmission schemes (i.e., unicast and broadcast) and we verify that the simulation results strictly follow our analysis, while the small deviation is due to the approximation of  $p_a$  and the tight bound used for the other clusters interference in the cluster coverage. Furthermore, we observe that the connectivity in broadcast scenarios is significantly higher than the connectivity in unicast transmissions, as it is more probable to successfully deliver a message in a random receiver around the transmitter than to a designated receiver due to the fading conditions.

Finally, in Fig. 13, we demonstrate the performance of the network in terms of connectivity for  $\nu = 1$ ,  $S = 5$  and  $\lambda_g = 0.02$ , while taking into account the solar harvesting performance for

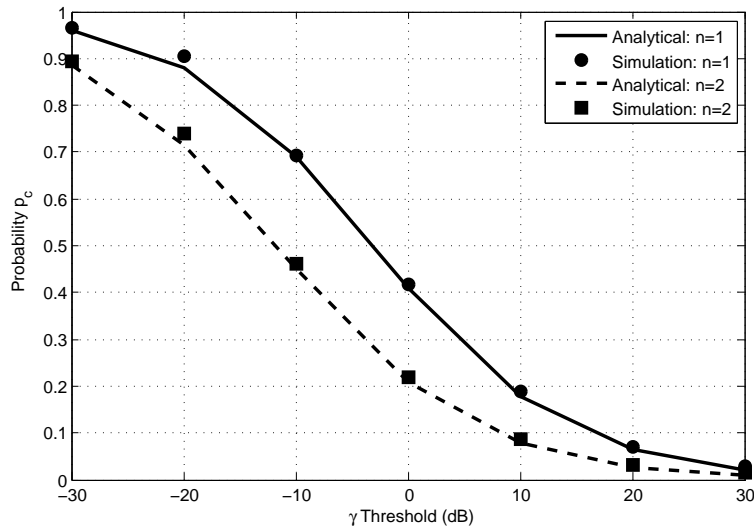


Fig. 11: Probability  $p_c$  vs.  $\gamma$  threshold for  $n = \{1, 2\}$ ,  $S = 5$ ,  $P_b = 30$  dBm and  $\nu = 1$ .

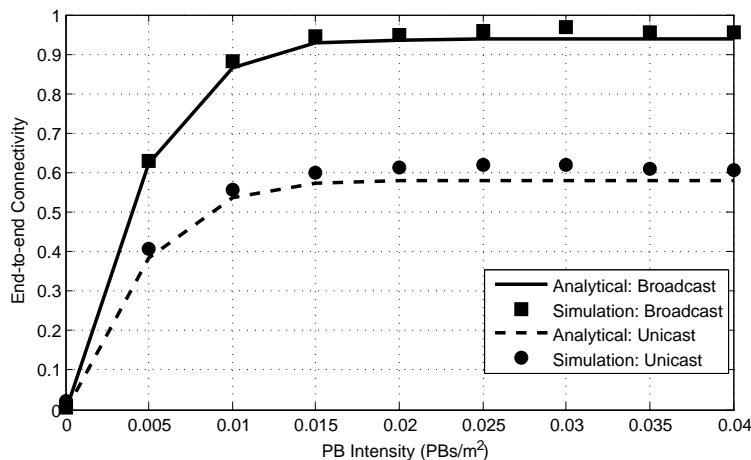


Fig. 12: End-to-end Connectivity vs. PB intensity  $\lambda_b$  for different transmission schemes for  $n = 1$ ,  $S = 5$  and  $\nu = 1$ .

the duration of one year. Similar to the PBs, the transmission power of the gateways depends on the solar harvesting performance. Hence, the connectivity performance varies according to the transmission scheme, the battery level and the decisions of the energy allocation algorithm. Therefore, in this figure, both the transmission power  $P_b$  of the PBs and  $P_g$  of the gateways are affecting the connectivity during the year. As we can observe, the connectivity in the unicast case (Fig. 13b) varies between 0.25 and 0.78, while for the broadcast case varies from 0.82 to 0.89 (Fig. 13c). This stems from the fact that in the unicast scheme, the GWs have to decode a message from their nearest GW and, thus, their transmission power affects the communication

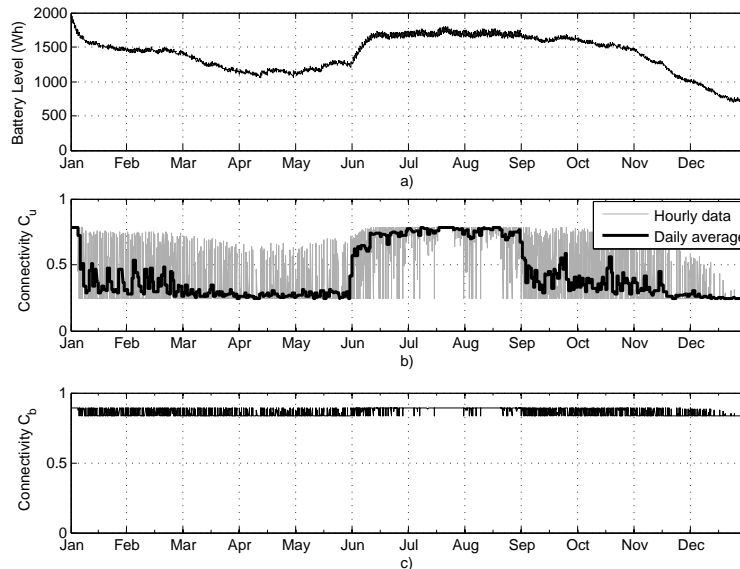


Fig. 13: Connectivity Probability vs. Time over the span of one year: a) Battery Level, b) Unicast, and c) Broadcast.

significantly. In contrast, in the broadcast case, the gateways decode the message with the strongest signal regardless of its proximity, resulting in a much higher connectivity ability.

## VII. CONCLUSION

In this paper, we studied the connectivity of a zero-energy WPSN under different transmission mechanisms (i.e., unicast, broadcast). For each scenario, we analytically derived the probability of connectivity, while considering the probability that the nodes are active. Moreover, we compared the different transmission mechanisms by assuming that battery-less nodes forming clusters harvest RF energy from PBs and showed that increasing the PB intensity is more beneficial for mission-critical applications than increasing the PB transmission power. As each PB and gateway is connected to a solar panel and a battery, we formulated a solar harvesting model and an energy allocation algorithm that adjusts the transmission power of PBs and gateways according to the cloud cover. We evaluated its performance and showed that the network operates without interruptions using only solar energy. Also, it has been shown that, under fading conditions, the broadcast scheme outperforms the unicast one. **In the future, we plan to extend this work in three ways: i) by implementing a testbed to acquire experimental data, ii) by employing variable RF-to-DC conversion efficiency in the model, which will provide more realistic results, and iii) by identifying the optimum solutions that provide full connectivity.**

## APPENDIX

## A. Derivations of Lemma 1

By taking the logarithm of (21), we obtain the Stirling's series

$$\ln(\Gamma(S)) = \left(S - \frac{1}{2}\right) \ln S - S + \frac{\ln(2\pi)}{2} + \sum_{\phi=1}^{\infty} \frac{B_{2\phi}}{2\phi(2\phi-1)S^{2\phi-1}} = \quad (40)$$

$$= \left(S - \frac{1}{2}\right) \ln S - S + \frac{\ln(2\pi)}{2} + \frac{1}{12S} - \frac{1}{360S^3} + \dots \quad (41)$$

where  $B_{2\phi}$  in (40) is a Bernoulli number. (41) can be given also as

$$\ln(\sqrt{S}\Gamma(S)) = S \ln S - S + \frac{\ln(2\pi)}{2} + \frac{1}{12S} - \frac{1}{360S^3} + \dots \quad (42)$$

Furthermore, we know from Euler's duplication formula that

$$\Gamma(S)\Gamma\left(S + \frac{1}{2}\right) = 2^{1-2S} \sqrt{\pi} \Gamma(2S). \quad (43)$$

Taking the natural logarithm of  $\Gamma\left(S + \frac{1}{2}\right)$  in (43) and employing (41), yields

$$\ln\left(\Gamma\left(S + \frac{1}{2}\right)\right) = S \ln S - S + \frac{\ln(2\pi)}{2} - \frac{1}{24S} + \frac{7}{2880S^3} + \dots \quad (44)$$

Subtracting (42) from (44), yields the approximate solution

$$\ln\left(\frac{\Gamma\left(S + \frac{1}{2}\right)}{\sqrt{S}\Gamma(S)}\right) = -\frac{1}{8S} + \frac{1}{192S^3} + \dots \quad (45)$$

Therefore,

$$\frac{\Gamma\left(S + \frac{1}{2}\right)}{\sqrt{S}\Gamma(S)} = \exp\left(-\frac{1}{8S}\right) \exp\left(\frac{1}{192S^3}\right) \dots \quad (46)$$

As  $S$  is a natural number both exponents in (46) are approximately 1 and it holds that

$$\frac{\Gamma\left(S + \frac{1}{2}\right)}{\Gamma(S)} \approx \sqrt{S}. \quad (47)$$

By replacing (47) in (11), we can reach the result of Lemma 1.

## B. Derivations of Lemma 2

To calculate this probability, we need first to define the distribution of the distances in a cluster both for the intra-cluster case, i.e., the distance between the sensors and the gateway, and the

inter-cluster case, i.e., the distance between the gateway and the other clusters on the plane. According to [8], the distribution of the distance between a random point in a cluster and the clusterhead is described by the Rayleigh distribution and it is given by

$$f_R(r, \sigma^2) = \frac{r}{\sigma^2} \exp\left(-\frac{r^2}{2\sigma^2}\right). \quad (48)$$

The probability  $p_c$  can be obtained by

$$p_c = p_a \mathbb{P}(\text{SIR} \geq \gamma) = p_a \mathbb{P}\left(hr^{-\alpha} \geq \frac{(I_{intra} + I_{inter})\gamma}{P_{tx}}\right). \quad (49)$$

By averaging the probability  $\mathbb{P}(\text{SIR} \geq \gamma)$  over the plane, we obtain

$$\mathbb{P}(\text{SIR} \geq \gamma) = \mathbb{E}[P(\text{SIR} > \gamma|r)] = \int_{r>0} P(\text{SIR} > \gamma|r) f_R(r) dr \quad (50)$$

$$= \int_{r>0} P(h > \gamma r^\alpha (I_{intra} + I_{inter})|r) f_R(r) dr \quad (51)$$

$$= \int_{r>0} \mathbb{E}_I[\exp(-\gamma r^\alpha (I_{intra} + I_{inter})|r)] f_R(r) dr \quad (52)$$

$$= \int_{r>0} \mathcal{L}_{intra}(\gamma r^\alpha) \mathcal{L}_{inter}(\gamma r^\alpha) f_R(r) dr, \quad (53)$$

where (52) follows from  $h \sim \exp(\mu)$ .

The number of interferers depends on the probability that these interferers will have enough power to be active during the CP. In this way, if some interferers have not received enough energy during the HP, they will not contribute at the total interference. To that end, the Laplace transforms for the intra-cluster  $\mathcal{L}_{intra}(s)$  and the inter-cluster  $\mathcal{L}_{inter}(s)$  interference provided in [8] are modified to take into account the active nodes with probability  $p_a$  and are given by

$$\mathcal{L}_{intra}(s) = \mathbb{E}\left[\exp\left(-s \sum_{f=1}^{\bar{n}p_a} h_f |w|^{-\alpha}\right)\right] = \mathbb{E}\left[\prod_{f=1}^{\bar{n}p_a} \frac{1}{1 + s|w|^{-\alpha}}\right] = \quad (54)$$

$$= \exp\left(-(\bar{n}p_a - 1) \int_0^\infty \frac{sw^{-\alpha}}{1 + sw^{-\alpha}} f_R(w, 2\sigma^2) dw\right). \quad (55)$$

For the Laplace transform of the inter-cluster interference  $\mathcal{L}_{inter}(s)$ , we follow the derivations provided in [8, Appendix F] to obtain

$$\mathcal{L}_{inter}(s) = \exp\left(-\frac{2\pi^2 \lambda_g \bar{n} p_a s^{2/\alpha}}{\alpha \sin(2\pi/\alpha)}\right). \quad (56)$$

Substituting (55) and (56) in (53), yields the result of Lemma 2.

## REFERENCES

- [1] C. Bockelmann *et al.*, “Massive machine-type communications in 5G: physical and MAC-layer solutions,” *IEEE Commun. Mag.*, vol. 54, no. 9, pp. 59-65, Sep. 2016.
- [2] N. Brahma *et al.*, “Deployment Strategies for Ultra-Reliable and Low-Latency Communication in Factory Automation,” in *Proc. IEEE Globecom*, Dec. 2015, San Diego, USA.
- [3] C. Bettstetter, “On the Minimum Node Degree and Connectivity of a Wireless Multihop Network,” in *Proc. ACM Mobihoc*, Jun. 2002, Lausanne, Switzerland.
- [4] D. Miorandi, E. Altman and G. Alfano, “The Impact of Channel Randomness on Coverage and Connectivity of Ad Hoc and Sensor Networks,” *IEEE Trans. Wireless Commun.*, vol. 7, no. 3, pp. 1062-1072, Mar. 2008.
- [5] P.-V. Mekikis *et al.*, “Connectivity of Large-Scale WSNs in Fading Environments under Different Routing Mechanisms,” in *Proc. IEEE ICC*, Jun. 2015, London, UK.
- [6] Haggai Roitman *et al.*, “Harnessing the crowds for smart city sensing,” in *Proc. ACM CrowdSens*, 2012, New York, NY.
- [7] X. Liu and Y. Ban, “Uncovering Spatio-Temporal Cluster Patterns Using Massive Floating Car Data,” *ISPRS International Journal of Geo-Information*, vol. 2, pp. 371-384, 2013.
- [8] M. Afshang, H. S. Dhillon and P. H. Joo Chong, “Modeling and Performance Analysis of Clustered Device-to-Device Networks,” *IEEE Trans. Wireless Commun.*, vol. 15, no. 7, pp. 4957-4972, July 2016.
- [9] T. Han and N. Ansari, “Powering mobile networks with green energy,” *IEEE Wireless Commun*, vol. 21, no. 1, pp. 90-96, Feb. 2014.
- [10] X. Lu *et al.*, “Wireless Networks With RF Energy Harvesting: A Contemporary Survey,” *IEEE Commun. Surveys Tutorials*, vol. 17, no. 2, pp. 757-789, Secondquarter 2015.
- [11] A. Boaventura *et al.*, “Optimum behavior: Wireless power transmission system design through behavioral models and efficient synthesis techniques,” *IEEE Microwave Mag.*, vol. 14, no. 2, pp. 26-35, Mar. 2013.
- [12] K. Huang and V. K. N. Lau, “Enabling Wireless Power Transfer in Cellular Networks: Architecture, Modeling and Deployment,” *IEEE Trans. Wireless Commun.*, vol. 13, no. 2, pp. 902-912, Feb. 2014.
- [13] D. Dondi *et al.*, “Modeling and Optimization of a Solar Energy Harvester System for Self-Powered Wireless Sensor Networks,” *IEEE Trans. Ind. Electron.*, vol. 55, no. 7, pp. 2759-2766, Jul. 2008.
- [14] C. Bergonzini, D. Brunelli and L. Benini, “Algorithms for harvested energy prediction in battery-less wireless sensor networks,” in *Proc. IWASI*, Jun. 2009, Trani, Italy.
- [15] C. Yang and K. W. Chin, “On complete targets coverage and connectivity in energy harvesting wireless sensor networks,” in *Proc. ICT 2015*, Sydney, NSW, 2015, pp. 391-397.
- [16] C. Wang *et al.*, “A hybrid framework combining solar energy harvesting and wireless charging for wireless sensor networks,” *IEEE INFOCOM 2016*, San Francisco, CA, 2016, pp. 1-9.
- [17] Y. Bao *et al.*, “Solar Radiation Prediction and Energy Allocation for Energy Harvesting Base Stations,” in *Proc. IEEE ICC*, Jun. 2014, Sydney, Australia.
- [18] D. Zhai *et al.*, “Leakage-Aware Dynamic Resource Allocation in Hybrid Energy Powered Cellular Networks,” *IEEE Trans. Commun.*, vol. 63, no. 11, pp. 4591-4603, Nov. 2015.
- [19] Y. L. Che, L. Duan and R. Zhang, “Spatial Throughput Maximization of Wireless Powered Communication Networks,” *IEEE J. Sel. Areas Commun.*, vol. 33, no. 8, pp. 1534-1548, Aug. 2015.
- [20] P.-V. Mekikis *et al.*, “Information Exchange in Randomly Deployed Dense WSNs with Wireless Energy Harvesting Capabilities,” *IEEE Trans. Wireless Commun.*, vol. 15, no. 4, pp. 3008-3018, Apr. 2016.

- [21] P.-V. Mekikis *et al.*, “Connectivity Analysis in Wireless-Powered Sensor Networks with Battery-less Devices,” in *Proc. IEEE Globecom*, Dec. 2016, Washington D.C., USA.
- [22] S. Bi, C. K. Ho, and R. Zhang, “Wireless powered communication: opportunities and challenges,” *IEEE Commun. Mag.*, vol. 53, no. 4, pp.117-125, Apr. 2015.
- [23] M. Haenggi, *Stochastic Geometry for Wireless Networks*, Cambridge University Press, 1st ed., 2013.
- [24] M. Haenggi *et al.*, “Stochastic geometry and random graphs for the analysis and design of wireless networks,” *IEEE J. Sel. Areas Commun.*, vol. 27, no. 7, pp. 1029-1046, Sep. 2009.
- [25] F. Baccelli, B. Blaszczyszyn, P. Muhlethaler, “Stochastic analysis of spatial and opportunistic aloha,” *IEEE J. Sel. Areas Commun.*, vol. 27, no. 7, pp. 1105-1119, Sep. 2009.
- [26] Federal Communications Commission, “Part 15: Radio Frequency Devices,” Code of Federal Regulations.
- [27] Insolation at 3-hourly intervals, *NASA Surface meteorology and Solar Energy*, Online: <https://eosweb.larc.nasa.gov/cgi-bin/sse/grid.cgi?>
- [28] N. Sharma, J. Gummeson, D. Irwin and P. Shenoy, “Cloudy Computing: Leveraging Weather Forecasts in Energy Harvesting Sensor Systems,” in *Proc. IEEE SECON*, Jun. 2010, Boston, MA.
- [29] L. W. Falls, “The Beta Distribution: A statistical model for world cloud cover,” *Geophysical Research*, vol. 79, no. 9, pp. 1261-1264, Mar. 1974.
- [30] R. Roth, “Comparison of Satellite and Surface Cloud Cover Observations and Cloud Cover Regions Over Europe,” *Climatology*, vol. 6, no. 4, pp. 327-337, Aug. 1988.
- [31] D. Stoyan, W. Kendall and J. Mecke, “Stochastic Geometry and Its Applications,” 2nd ed. John Wiley and Sons, 1996.
- [32] M.D. Penrose, “On  $k$ -connectivity for a geometric random graph,” *Wiley Random Structures and Algorithms*, vol. 15, no. 2, pp. 145-164, 1999.
- [33] E. S. Sousa and J. A. Silvester, “Optimum transmission ranges in a direct- sequence spread-spectrum multihop packet radio network,” *IEEE J. Sel. Areas Commun.*, vol. 8, pp. 762-771, Jun. 1990.
- [34] M. Villarrubia, A. Coronas and M. Llorens, “Solar Radiation Incident on Tilted Flat Surfaces in Barcelona, Spain,” *Solar Energy*, vol. 25, no. 3, pp. 259-263, 1980.
- [35] Whisper by Talk<sup>2</sup> datasheet. Online: <https://bitbucket.org/talk2/whisper-node-avr>
- [36] ESP8266EX datasheet. Online: <http://download.arduino.org/products/UNOWIFI/0A-ESP8266-Datasheet-EN-v4.3.pdf>
- [37] M. Zorzi and S. Pupolin, “Outage probability in multiple access packet radio networks in the presence of fading,” *IEEE Trans. Veh. Tech.*, vol. 43, no. 3, pp. 604-610, Aug. 1994.